

Field and Service Robotics: Homework 4

Giulio Acampora P38000258

This document contains the Homework 4 of the Field and Service Robotics class. The GitHub link is
https://github.com/GUM-i-R0/FSR_Homework4.git

Contents

POINT 1	3
POINT 2	3
POINT 3	3
Trot, Trot Run, and Crawl	4
Bound, Pacing, and Gallop	6
Trot Comparisons	8
POINT 4	11
Leg Length	13
Inter-Leg Angle	15
Slope Inclination	16

POINT 1

The buoyancy effect appears when a rigid body is submerged in a fluid under the effect of gravity, as a buoyancy upward force that directly opposes the weight of the body. It is a hydrostatic effect, meaning it appears even when the robot is not moving, since it is not a function of the relative movement between the body and the fluid. In particular, it is given by Archimedes' principle:

$$b = \rho \Delta ||\bar{g}||$$

where ρ is the density of the fluid, Δ is the volume of the body, and \bar{g} is the gravity vector. The main difference regarding this effect between underwater robots and aerial robots is the difference in the density of the fluid. Water is much denser than air; that's why in underwater robotics it must be considered, while in aerial robotics it can often be neglected. In particular, it must be considered also because, in general, the center of gravity and the center of buoyancy can be different. When designing an underwater robot, it is important that the center of buoyancy and the center of mass are at least aligned on the same vertical line (of course in opposite directions), otherwise, when using adaptive controllers, there could be large induced torques to compensate even small displacements between the two centers.

POINT 2

- a. **FALSE**, the added mass must not be considered as an additional load but rather as an inertial contribution. It is a hydrodynamic effect that arises when a rigid body is moving in a fluid that is accelerated by the movement of the body. That's why it cannot be considered as just an additional load: it arises only when there is acceleration. The effect is like a virtual reaction force in the opposite direction that tries to counteract the motion and is considered in the dynamic model with a change in the mass matrix and in the Coriolis matrix.
- b. **TRUE**, unlike the case of aerial or legged robots where the air density is much lower than the density of the moving robot and where instead the effect can be neglected.
- c. **TRUE**, the damping effect is the sum of two forces proportional to the velocity in the opposite direction. These are due to the viscosity of the fluid and are dissipative forces, leading to a contribution to stability.
- d. **FALSE**, the ocean current is usually modeled as a constant velocity contribution with zero acceleration when expressed in the world frame, and so it is better to not refer to it with respect to the body frame, because in this case you would have to consider the relative velocity v_r that is not constant and is configuration dependent.

POINT 3

The quadratic function using the QP solver qpSWIFT has been implemented in the `MAIN.m` Matlab script. To obtain comparable plots for different parameters, the resulting data have been saved and then loaded in the `report_plot.m` Matlab script.

The videos taken can be viewed at https://github.com/GUM-i-RO/FSR_Homework4.git.

First, various gaits for the quadruped robot have been simulated. For these simulations, a robot with a reasonable nominal mass was considered, designed to move only in the heading direction without changing its attitude, and moving on a high-friction plane surface like dry concrete. The center of mass (CoM) is located at a height of 0.2 m, and the simulation duration is 4.5 seconds.

Nominal values:

- Mass of the robot $m = 5.5$ kg
- Desired velocity $\dot{p}_{c,x \text{ ref}} = 0.5$ m/s

- Friction coefficient $\mu = 1$

The chosen gait affects not only the motion via the foot scheduler and how the stance feet sequence changes, but also the stability, as it alters the shape of the support polygon.

Six different types of gait have been analyzed. For each, the time histories of the CoM coordinates ($p_{c,x}$, $p_{c,y}$, $p_{c,z}$), the linear velocities ($\dot{p}_{c,x}$, $\dot{p}_{c,y}$, $\dot{p}_{c,z}$), the angular velocities of roll ($\dot{\varphi}$), pitch ($\dot{\theta}$), and yaw ($\dot{\psi}$), and also the vertical ground reaction forces ($f_{gr,z}$) of all four legs (left/right front/hind) have been plotted and discussed. Furthermore, videos for each gait are attached and it is advised to watch them while reading this report to better visualize the robot's motion. To better summarize and compare the results in the report, the gaits "trot", "trot run", and "crawl" have been plotted together. The same will be repeated later for the gaits "bound", "pacing", and "gallop".

Trot, Trot Run, and Crawl

The "trot" gait is characterized by the simultaneous lifting and swinging forward of diagonally opposite pairs of feet, which are then placed back on the ground. During the sequence, there is a short phase where all four legs are on the ground, increasing the effective stability.

The "trot run" gait is quite similar, with the difference that there is no phase with all legs on the ground; as soon as the swing legs become stance legs, the current stance legs become swinging. This increases the tracking performance for velocity, but as a trade-off, stability degrades.

The "crawl" gait is characterized by lifting only one leg at a time, ensuring that at least three legs remain in continuous contact with the ground. This results in the most stable gait, as the support polygon will remain at least a triangle at all times.

In Fig. 1, you can observe from $p_{c,x}$ how the robot successfully follows the desired trajectory in all three cases while maintaining appreciable stability. This is indicated by the minimal oscillations in $p_{c,y}$ and $p_{c,z}$, with the exception of the "trot run" gait which, as anticipated, is not able to fully recover its position along the vertical axis.

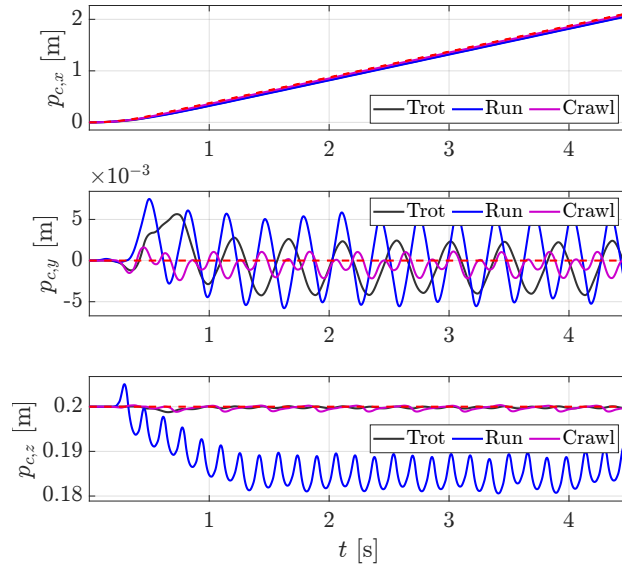


Figure 1: CoM coordinates with Trot, Trot run and Crawl gaits.

The same insights can be gained by looking at the linear velocities in Fig. 2, where oscillations provide insights into the robot's lateral stability and the vertical "bounciness" characteristic of the gait. Here, you can clearly see how the "trot run" gait is the most effective at following the $\dot{p}_{c,x}$ velocity reference. The

attitude plot in Fig. 3 shows the good postural stability of all three gaits, meaning the torso maintains a consistent orientation throughout the duration. This is particularly useful if the robot needs to carry a load.

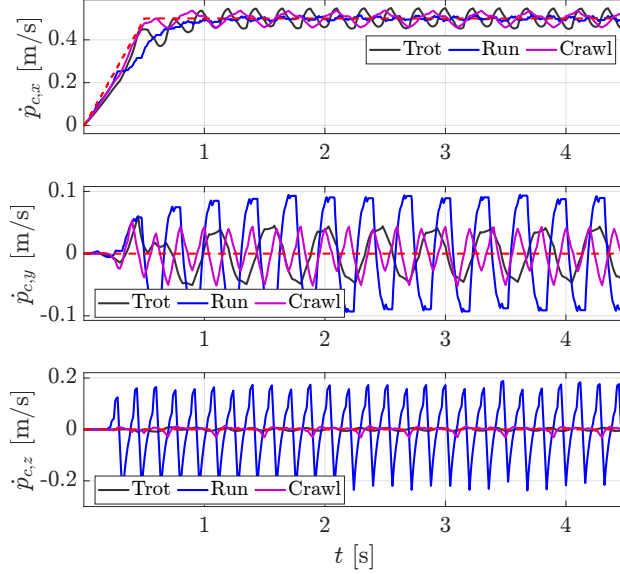


Figure 2: Linear Velocities with Trot, Trot run and Crawl gaits.

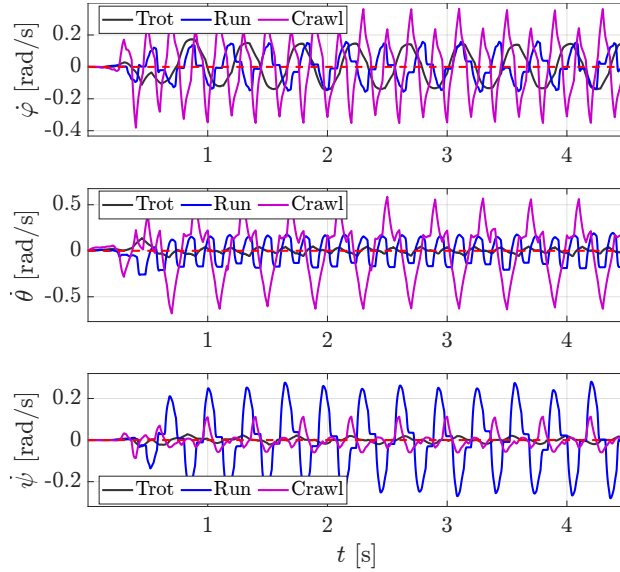


Figure 3: Angular Velocities with Trot, Trot run and Crawl gaits.

In Fig. 4, the ground reaction forces along the vertical axes are shown. By observing how forces are distributed among the supporting legs and identifying when forces are zero, one can understand which leg is swinging, thereby capturing the sequence and force distribution pattern. For the "trot" gait, you can see synchronized load sharing between diagonal pairs of legs, with the sequence being: left front/right hind \rightarrow right front/left hind. The same pattern holds for the "trot run" gait, but with no phase where all forces are equal to zero. For the "crawl" gait, a continuous exchange between stance legs is evident, and the sequence is particularly clear: left front \rightarrow right front \rightarrow left hind \rightarrow right hind.

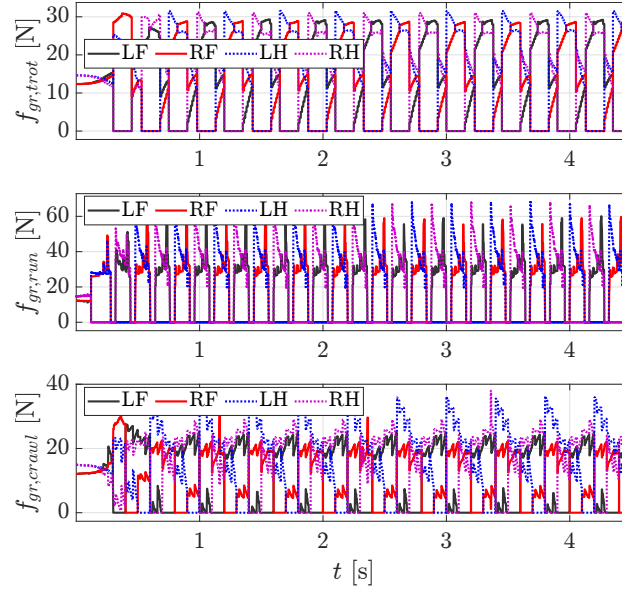


Figure 4: Ground Reaction Forces with Trot, Trot run and Crawl gaits.

Bound, Pacing, and Gallop

The "bound" gait is a running gait characterized by alternating support between pairs of legs, with the front and hind legs acting in unison to propel the body forward.

The "pacing" gait is another dynamic gait where the two legs on the same side of the robot move in unison. The "gallop" gait is a high-speed running gait, characterized by an asymmetric leg coordination pattern where typically only one leg is on the ground for each step.

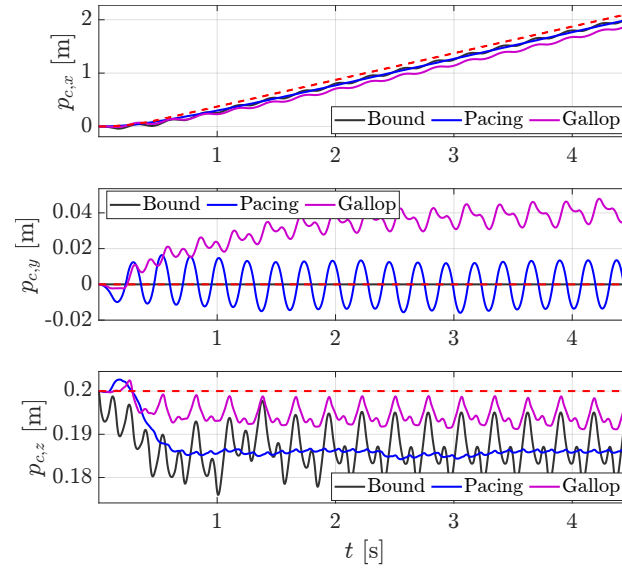


Figure 5: CoM coordinates with Bound, Pacing and Gallop gaits.

In these cases, as seen in Fig.5 from $p_{c,x}$, the reference is still tracked, but with greater difficulty compared to the previous gaits. Regarding the velocity $\dot{p}_{c,x}$ in Fig.6, you can clearly see how the "bound" and "gallop" gaits are forced to move back and forth to accommodate the relatively low desired velocity (this is even

clearer if you look at the attached videos). This presents a problem, especially during the slow transient phase, since these gaits are intended for high-velocity tracking and perhaps should be used with some form of gait switching. In fact, for the "gallop" gait, observing $p_{c,y}$ reveals a lateral offset that is not recovered, suggesting some instability. Something particular is shown by $p_{c,y}$ and $\dot{p}_{c,y}$ of the "bound" gait, which are characterized by perfect tracking without any oscillations; this could be very useful for specific tasks.

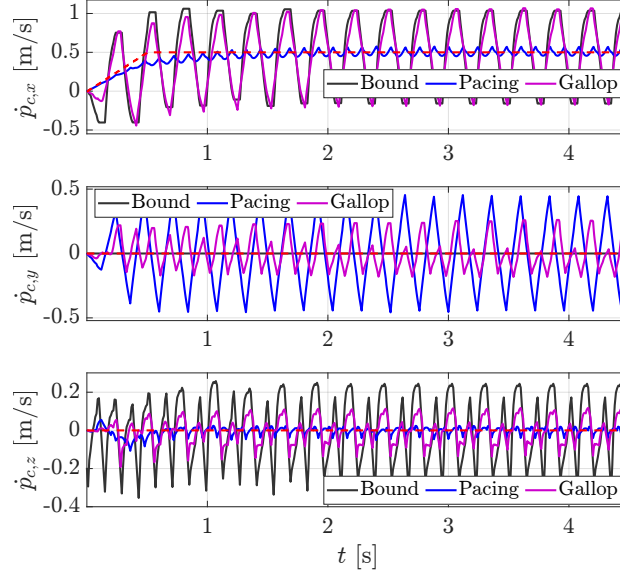


Figure 6: Linear Velocities with Bound, Pacing and Gallop gaits.

The increased angular velocity oscillations from Fig.7 directly indicate that the motion becomes more dynamic compared to the previous gaits.

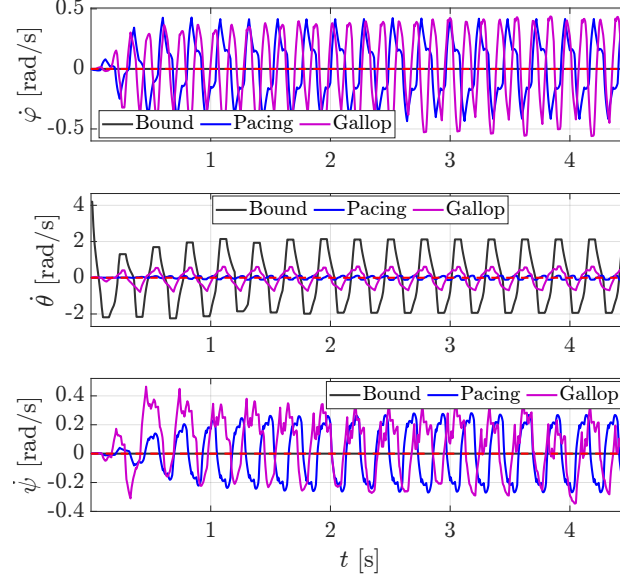


Figure 7: Angular Velocities with Bound, Pacing and Gallop gaits.

Again, by observing how ground reaction forces are distributed among the supporting legs in Fig.8, one can understand the sequence of steps. For the "bound" gait, synchronized f_{gr} peaks from the front and hind legs

acting in unison are visible, and a distinct "flight phase" (where all feet are simultaneously off the ground) is observable, manifesting as periods of zero vertical f_{gr} . The sequence, as anticipated, is left front/right front → left hind/right hind. For the "pacing" gait, the synchronized forces are from the right and left legs, and the sequence is left front/left hind → right front/right hind. For the "gallop" gait, it is easier to understand which leg is not swinging from the peaks; the sequence is left front → right front → left hind → right hind. Additionally, higher and more impulsive peaks are evident, which might suggest increased mechanical stress on the robot's limbs and joints.

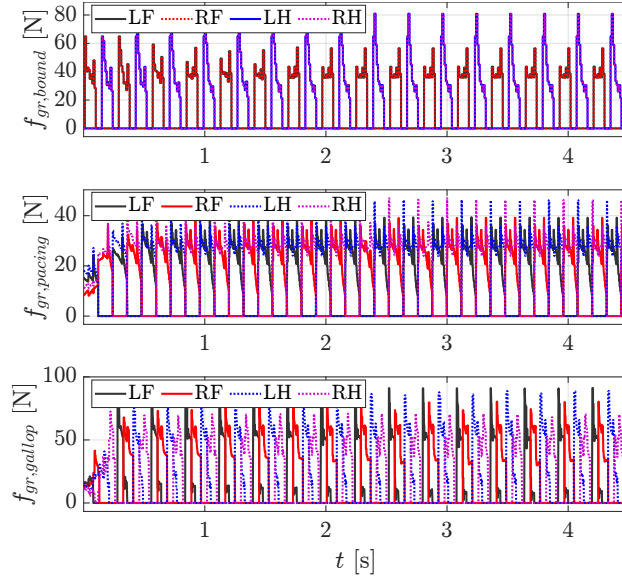


Figure 8: Ground Reaction Forces with Bound, Pacing and Gallop gaits.

Trot Comparisons

To further analyze how the motion is affected by the parameters, a change in robot mass and friction coefficient was performed, maintaining all other parameters as before and focusing on the "trot" gait, which is the more standard one.

First, different values for the robot's mass have been compared. In addition to the nominal 5.5 kg used in previous cases, two more values have been added: half (2.75 kg) and double (11 kg) the nominal mass.

The CoM coordinates are shown in Fig.9. Here, you can observe how the vertical $p_{c,z}$ in particular is affected, as expected, since increased inertia will mean that it will be harder to recover from larger, more sustained disturbances.

Furthermore, an increased robot mass will predictably lead to higher vertical f_{gr} since these counteract gravity, providing the necessary support to hold the robot's weight. This can be clearly seen in Fig.10, where the scaling with mass is evident. This would lead to increased energy consumption and also stress on the legs. The compared velocities are not shown because they appear to be very similar, thus not adding anything meaningful to this report.

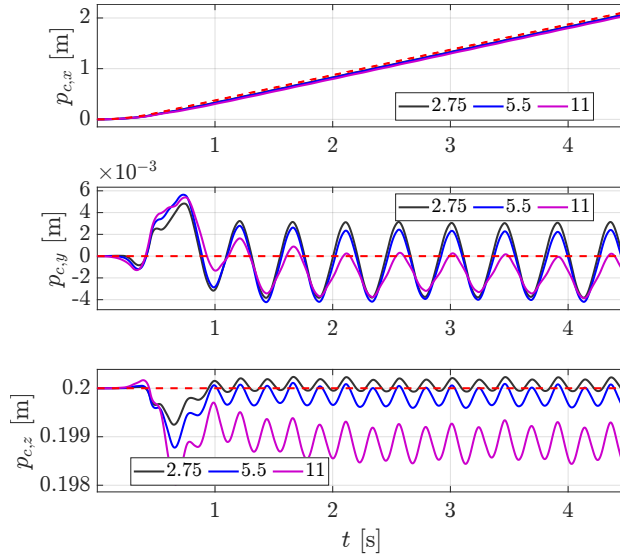


Figure 9: CoM coordinates with different values of robot mass.

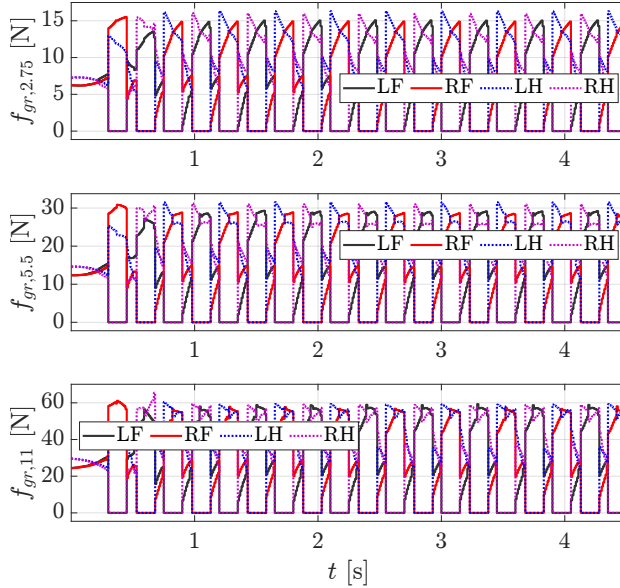


Figure 10: Ground Reaction Forces with different values of robot mass.

After this, different values for the friction coefficient have been compared. In addition to the nominal 1 from previous cases, two more values have been added: 0.05 to simulate an ice surface and 0.5 to simulate wet asphalt.

The results are compared in Figs.11, 12, and 13. You can see how the cases of wet and dry asphalt look almost the same, while the critical case is the ice one. In particular, from $\dot{p}_{c,x}$, you can see that the robot struggles to maintain its desired linear velocity during the acceleration phase, and from $\dot{p}_{c,z}$, you can observe increased vertical bouncing. From the angular velocities, it is clear how the postural stability decreases significantly. From the ground reaction forces, you can see how the values are clearly different, reflecting the fact that the robot's ability to generate propulsive or braking forces diminishes.

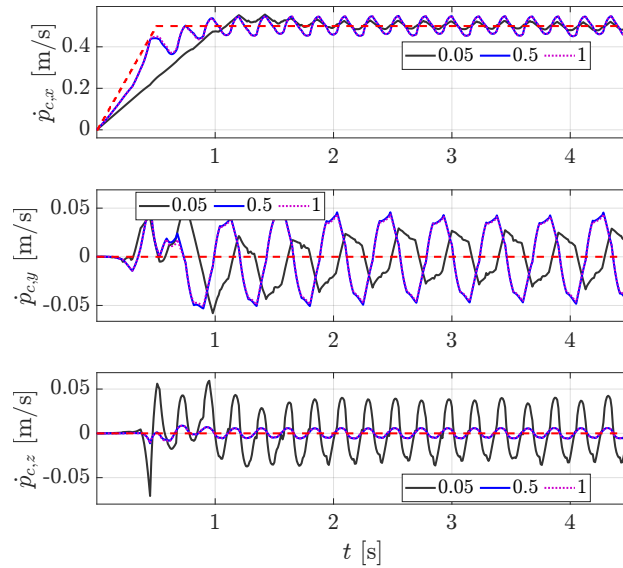


Figure 11: Linear Velocities with different values of friction coefficient (ice, wet and dry concrete).

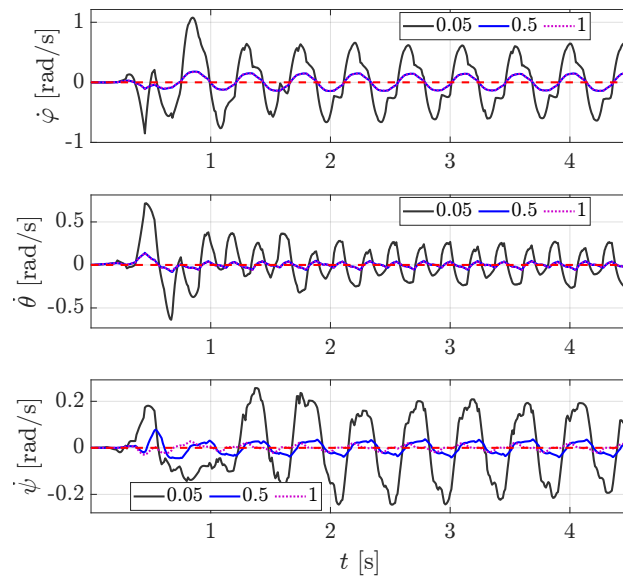


Figure 12: Angular Velocities with different values of friction coefficient (ice, wet and dry concrete).

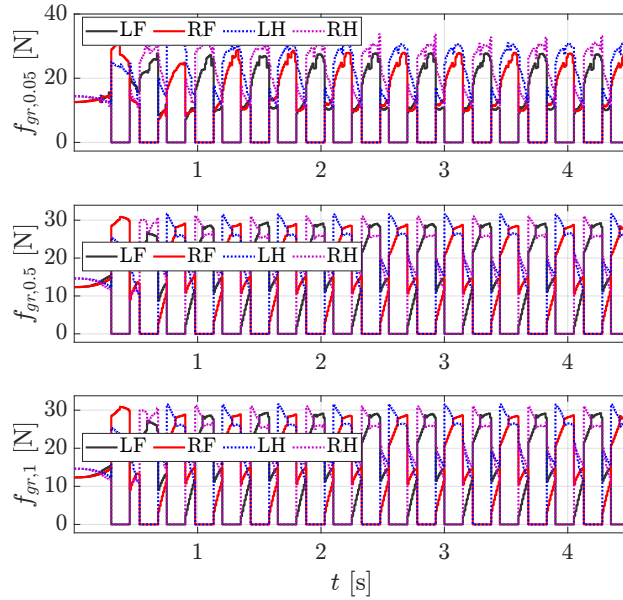


Figure 13: Ground Reaction Forces with different values of friction coefficient (ice, wet and dry concrete).

POINT 4

The Matlab file `rimless_wheel.m`, which simulates the motion of a rimless wheel, has been duplicated and modified to obtain different and comparable results. First, a preliminary analysis of the system's fixed points is performed by varying only the initial angular velocity $\dot{\theta}_0$ while maintaining all other parameters at their nominal values:

- Leg length $l = 1.0$ m
- Half inter-leg angle $\alpha = \pi/8$ rad
- Slope angle $\gamma = 0.08$ rad

After several simulations, it has been observed that the system will either converge to a stable equilibrium point or to a stable limit cycle.

The equilibrium point is characterized by zero angular velocity and a constant angular position. This represents an angle where the wheel is at rest and is stably balanced on two feet. More precisely, in simulation, there are two distinct angular positions:

$$\begin{aligned}\theta_1 &= \gamma - \alpha \\ \theta_2 &= \gamma + \alpha\end{aligned}$$

These are the two values for which the impact event occurs (i.e., the next foot touches the ground). However, they appear distinct only due to how the system is modeled; in reality, they correspond to the same physical standing point. Therefore, for the following analysis, they are considered to represent the same equilibrium. The limit cycle is a stable periodic solution that corresponds to a consistent, continuous, and self-sustained walking gait. This occurs thanks to a precise balance between the energy gained from gravity during each step and the energy dissipated after impacts with the ground. Forward walking for $\dot{\theta}_0 > 0$ (in the downward direction) is relatively straightforward to understand and consistently occurs when the initial velocity $\dot{\theta}_0$ is greater than a threshold ω_1 :

$$\omega_1 = \sqrt{\frac{2g}{l}(1 - \cos(\gamma - \alpha))} \quad (1)$$

This ω_1 represents the minimum kinetic energy threshold required for the system to successfully take a step. Its dependence on various parameters will be analyzed in more detail in the next section.

The same predictability cannot be applied to $\dot{\theta}_0 < 0$ (in the upward direction). Here, it is not immediately clear for which initial angular velocities the robot will achieve a walking gait and for which it will stand still. Even if we consider an analogous threshold:

$$\omega_2 = -\sqrt{\frac{2g}{l}(1 - \cos(\gamma + \alpha))} \quad (2)$$

at which the system is theoretically able to take a step in the upward direction.

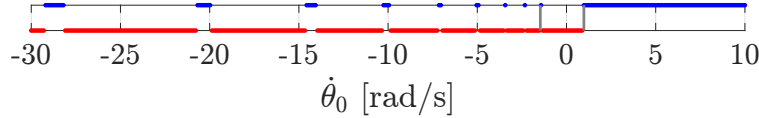


Figure 14: Basins of attraction of equilibrium point (red) and limit cycle (blue).

In Fig. 14, the basins of attraction are shown for different positive and negative values of $\dot{\theta}_0$. The blue dots represent initial conditions for which the system trajectories eventually converge towards the limit cycle, while the red dots represent those that converge towards the equilibrium point. ω_1 and ω_2 are indicated by grey lines. As anticipated, to achieve the walking gait for positive $\dot{\theta}_0$, it simply needs to be greater than ω_1 . For negative $\dot{\theta}_0$, the intervals of blue values become sparse and less clearly defined. Interestingly, these intervals become larger as the magnitude of $\dot{\theta}_0$ (in the negative direction) increases.

For detailed plot analyses, four different values of $\dot{\theta}_0$ were chosen: -3 rad/s, -1.42 rad/s, 0.95 rad/s, and 3 rad/s.

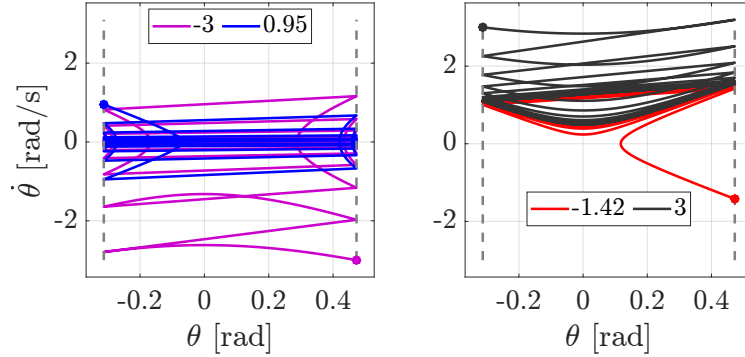


Figure 15: Phase portraits with different values of initial angular velocities.

In Fig. 15, the phase portraits are shown. You can observe how, when θ reaches the value $\gamma + \alpha$ (the right grey dashed line), indicating a "step," it instantaneously jumps back to $\gamma - \alpha$ (the left grey dashed line) with a lower $\dot{\theta}$ (due to energy dissipation from the impact with the ground). Notice how, in the plot on the right, the system converges to the exact same limit cycle even though the initial conditions (black and red dots) are significantly different.

This behavior is better visualized in Fig. 16, which shows the time histories of the angular position θ . Again, you can see how it jumps back and forth between $\gamma + \alpha$ and $\gamma - \alpha$ (grey dashed lines). Particularly, in the top plot, it shows an "infinite" frequency until it stops, while in the bottom plot, you can see periodic motions that converge to exactly the same frequency (they overlap each other).

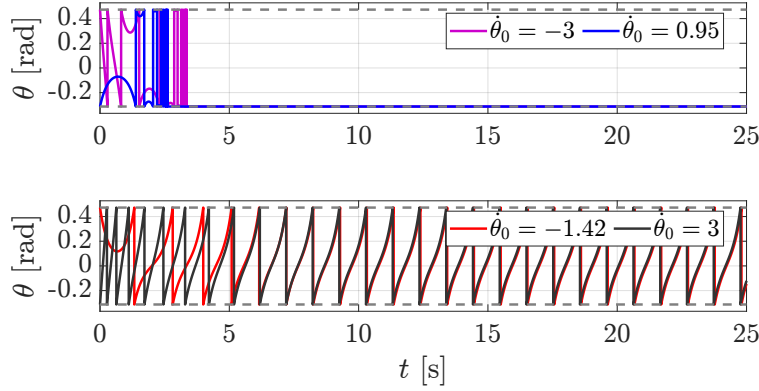


Figure 16: Time histories of angular position with different values of initial angular velocities.

In Fig. 17, the time histories of the angular velocity $\dot{\theta}$ are shown. ω_1 and ω_2 are also depicted as dashed grey lines. You can observe how the walking gait is achieved only when $\dot{\theta}$ overcomes, in some manner, the threshold ω_1 . It is interesting that even if the initial push is much larger (e.g., $\dot{\theta}_0 = 3 \text{ rad/s}$), the system will initially slow down until it reaches the same walking gait with a velocity that oscillates around ω_1 .

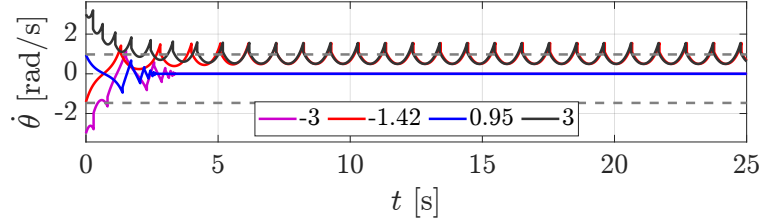


Figure 17: Time histories of angular velocity with different values of initial angular velocities.

Now, as anticipated, the effect of each parameter on the system's trajectories will be analyzed, maintaining the initial angular velocity constant at $\dot{\theta}_0 = 0.95 \text{ rad/s}$.

Leg Length

The effect of changing the leg length l is primarily related to the threshold ω_1 .

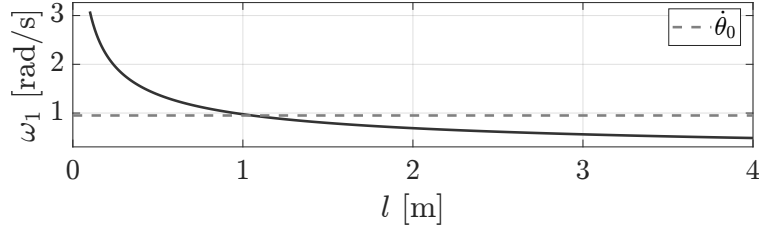


Figure 18: Relationship between angular velocity threshold and leg length.

In Fig. 18, you can see how ω_1 changes with respect to l ; specifically, it is inversely proportional to the square root of l . This indicates that increasing the leg length will result in a lower initial push needed to sustain walking.

You can also compute the minimum value for the leg length using the inverse formula:

$$l_{\min} = \frac{2g}{\dot{\theta}_0^2} (1 - \cos(\gamma - \alpha)) \quad (3)$$

With $\dot{\theta}_0 = 0.95 \text{ rad/s}$, this yields $l_{\min} = 1.0542 \text{ m}$. Four different values of l have been analyzed: 0.1 m, 1 m, 1.06 m, and 10 m. The first two cases (0.1 m, 1 m) will converge to the equilibrium point, while the latter two (1.06 m, 10 m) will converge to a limit cycle.

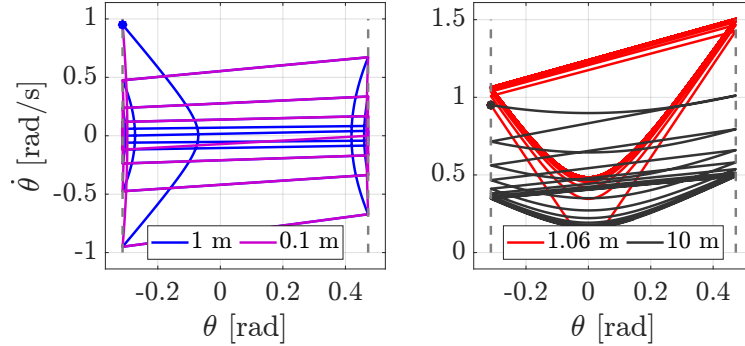


Figure 19: Phase portraits with different values of leg length.

In Fig. 19, the phase portraits are shown. From the plot on the right, you can see how increasing l results in a limit cycle that is lower (due to lower velocities) and more "flattened."

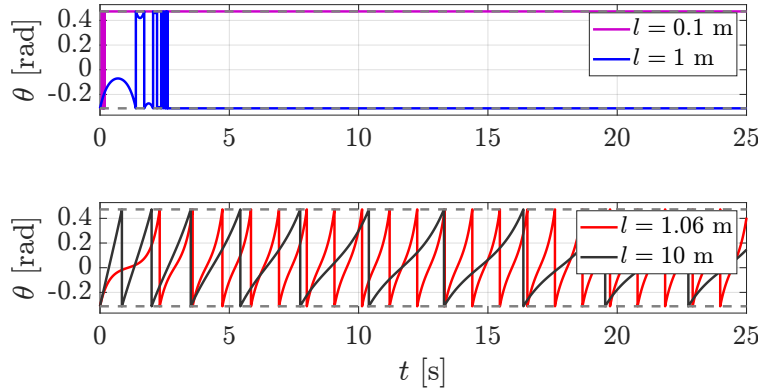


Figure 20: Time histories of angular position of θ with different values of leg length.

In Fig. 20, you can see the time histories of θ and understand how the frequencies of motion are now different, unlike the previous case, due to the "longer" steps.

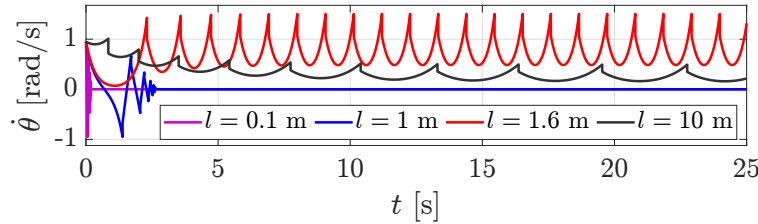


Figure 21: Time histories of angular velocity of $\dot{\theta}$ with different values of leg length.

This is even more evident if you look at the time histories of $\dot{\theta}$ shown in Fig. 21, where you can observe that the longer the legs, the slower the steps will be.

Inter-Leg Angle

Changing the inter-leg angle α is a bit more interesting. If α is lower than the slope inclination γ , then the conditions for the equilibrium point disappear, and only the limit cycle is possible.

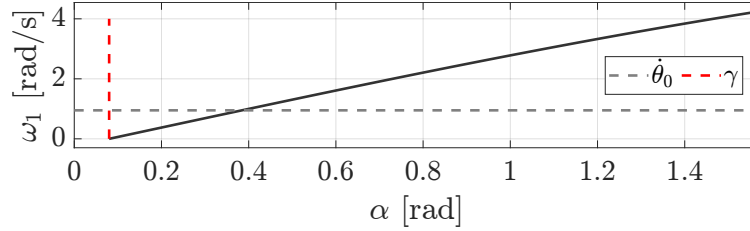


Figure 22: Relationship between angular velocity threshold and inter-leg angle.

In Fig. 22, how ω_1 changes with respect to α is shown, with α varying from γ to $\pi/2$. You can see how ω_1 is proportional to α , and also that when $\alpha = \gamma$, then $\omega_1 = 0$. Four different values of α have been analyzed: $\pi/16$ rad, $\pi/12$ rad, $\pi/8$ rad, and $\pi/6$ rad.

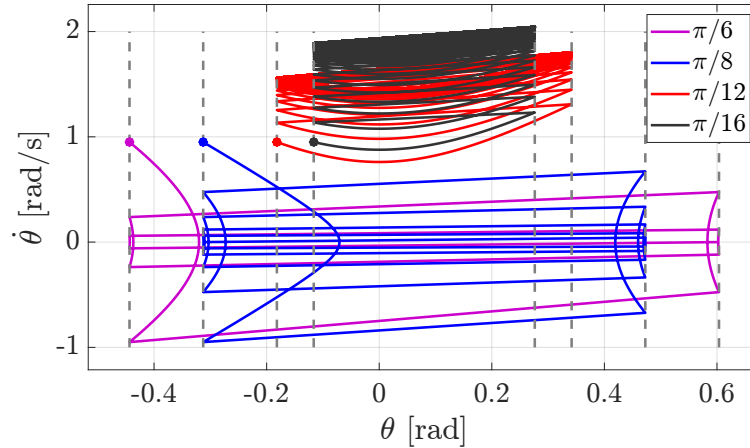


Figure 23: Phase portraits with different values of inter-leg angle.

In Fig. 23, the phase portraits are shown. You can see that the smaller the inter-leg angle α is, the slimmer the limit cycle will be, as expected by the fact that its angular range lives between $\gamma - \alpha$ and $\gamma + \alpha$.

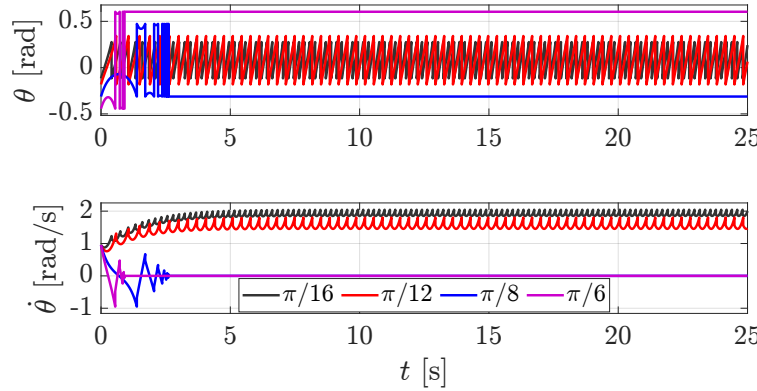


Figure 24: Time histories of states with different values of inter-leg angle.

In Fig. 24, the time histories of the states are shown. Now you can observe that the smaller α is, the more frequent the steps will be.

Slope Inclination

As anticipated in the previous section, if the slope inclination angle γ is greater than α , then only a limit cycle is possible.

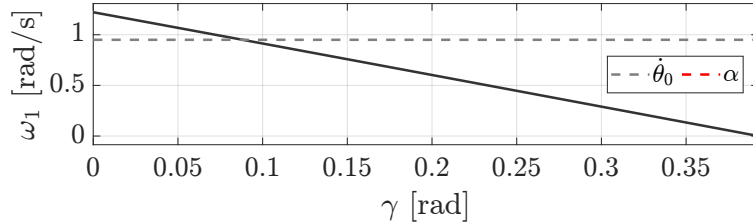


Figure 25: Relationship between angular velocity threshold and slope angle.

In Fig. 25, you can see how ω_1 changes with respect to γ , with γ varying between 0 and α . Here, ω_1 is inversely proportional to γ , and when $\gamma = \alpha$, then $\omega_1 = 0$. Thus, increasing γ will result in a lower velocity needed to walk, which is intuitive as the slope becomes steeper. Four different values of γ have been analyzed: 0 rad, 0.08 rad, 0.16 rad, and 0.24 rad.

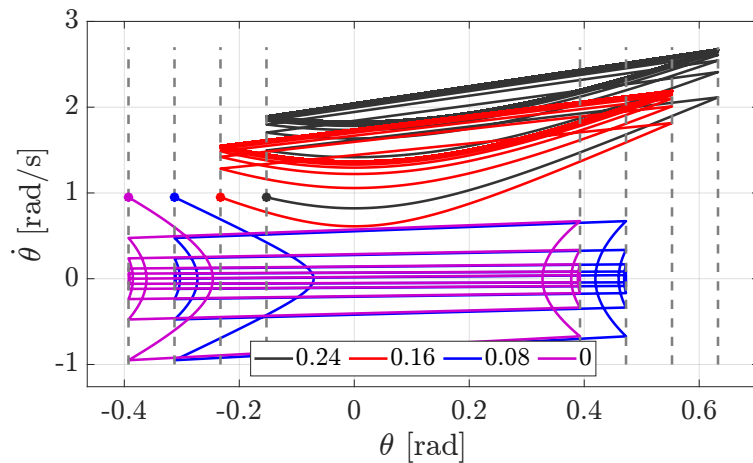


Figure 26: Phase portraits with different values of slope angle.

In Fig. 26, the phase portraits are shown. You can see how increasing γ shifts the entire phase plane to the right. Considering that the underlying phase plane is that of an inverted pendulum, this shifting moves the portrait into a region where the energy gained from gravity is greater.

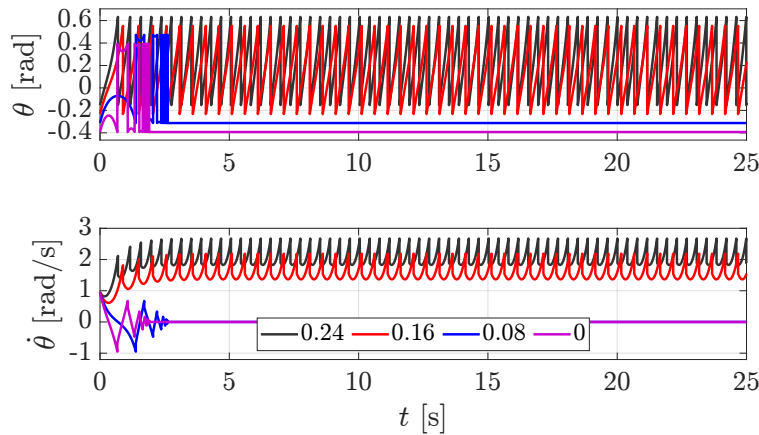


Figure 27: Time histories of states with different values of slope angle.

From Fig. 27, you can see the time histories of the states. Now, the frequency of each step is the same, but the velocity magnitude is greater, as the slope becomes steeper.